Abnormal staircase-like I-V curve in InGaN quantum well solar cells

X. M. Cai,[1] Z. W. Zheng,[2] H. Long,[2] L. Y. Ying,[2] and B. P. Zhang[2,a)]
[1]*Department of Physics, Jimei University, Xiamen 361021, Fujian, People's Republic of China*
[2]*Optoelectronics Engineering Research Center, Department of Electronic Engineering, Xiamen University, Xiamen 361005, Fujian, People's Republic of China*

(Received 7 December 2017; accepted 29 March 2018; published online 17 April 2018)

InGaN/GaN multiple quantum well-solar cells with different barrier thicknesses have been comparatively studied, and it is demonstrated that a thinner barrier facilitates the transport of photogenerated carriers. Meanwhile, an abnormal but regular staircase-like *I-V* curve is observed. The induction factors and microscopic physical process relevant to this abnormal feature are analyzed in detail, which is found closely related to the inadequate internal field and special epitaxial structure. Furthermore, the formation conditions of *I-V* curves with various types of inflections are also proposed. This work provides insight into the origin of device problems, which can be applicable to other types of solar cells. *Published by AIP Publishing.* https://doi.org/10.1063/1.5018481

The III nitride semiconductor InGaN has recently drawn intensive research interest due to its favorable physical properties and unique advantage of direct and tunable bandgap (0.64–3.42 eV) that matches perfectly the solar spectrum. The single ternary alloy system, stacked InGaN subcells with an adjustable indium (In) composition, has the potential to form a full-solar-spectrum high-efficiency photovoltaic device[1] that can work not only under normal conditions but also in severe environments.[2,3] The InGaN alloy ($E_g > 2.5$ eV) is also a good candidate that can be incorporated in the multijunction tandem cell to achieve power conversion efficiency greater than 50%.[4] Although a promising future is ahead, InGaN-based solar cells (SCs) are still at their infancy, and many obstacles need to be overcome. The most challenging is to achieve a thick high-quality InGaN layer with a desired In composition, which suffers from the lack of the native substrate and lattice mismatch between InGaN/GaN heterolayers. The undesirable structure defects can easily form in the InGaN epilayer, which reduce the lifetime of photogenerated carriers[5] and thus degrade the photovoltaic performance.[6] An alternative strategy was proposed to use the InGaN/GaN multiple quantum well (MQW) as the intrinsic region to relieve the lattice-mismatch, which was demonstrated to play a positive role in InGaN SCs.[7,8] Nevertheless, carrier confinement still remains, restricting the transport of photogenerated carriers in MQW-SCs. Another challenge is to obtain a sufficient p-type doping in III-nitride alloys by lowering the influence of the high background electron concentration and low Mg activation efficiency[9,10] in that the effective p-type doping is a determining factor for the strength of the built-in electric field (E_{bi}) of a p-n junction. Besides, in the III nitride material system grown on a c-plane sapphire substrate along the (0001) direction, there exists a large polarization induced field that has detrimental effects on the separation of photogenerated carriers.[11]

The current-voltage (*I-V*) characteristic is an important indicator for directly evaluating solar cell performance. Instead of the expected "square" shape *I-V* curve, in certain cases, the unexpected "staircase" shape appears, which lowers the fill factor (*FF*), even the short circuit current density (J_{sc}) or open circuit voltage (V_{oc}), and thus reduces the performance of the solar cell. This abnormal case had been reported previously in the actual or modelled solar cells;[11–14] however, the specific reason was not mentioned. Li *et al*. first theoretically demonstrated that this staircase behavior can be caused by polarization charges that have detrimental effects on the collection of photogenerated carriers.[15] This proposal was confirmed by other theoretical studies.[16–20] Through experiment, Neufeld *et al*. showed that the polarization charges can be screened by sufficient doping.[11] Despite these studies, the investigation on the contributing factors and underlying physical process of the abnormal behavior, especially the multiple staircases (shown in Fig. 2), is still lacking.

In this work, we investigate the InGaN/GaN MQW-SCs and focus on analysing an abnormal staircase-like *I-V* curve. The relevant cause and physical process of such an abnormal feature are studied, and the required conditions for various types of inflections are also analysed. The results presented here can be extended to more applications, and an improvement of device design can be expected.

InGaN MQW samples were grown on c-plane sapphire substrates by Thomas Swan low-pressure metalorganic chemical vapor deposition (MOCVD). The epitaxial structure is as follows: a 2-μm Si-doped n-GaN layer was grown on a 25-nm low-temperature GaN buffer layer, and subsequently, ten-periods of InGaN/GaN MQWs with an intentional low n-doped (10^{17} cm^{-3}) barrier were grown as the main absorption region; 150-nm Mg-doped p-GaN was finally capped to serve as the window layer. The structure parameters for the MQW region are depicted in Fig. 1. The electron concentration in n-GaN was estimated to be approximately 5×10^{18} cm^{-3}, and the hole concentration in p-GaN was approximately 7×10^{16} cm^{-3}. The mesa size of MQW-SCs was designed to be 1 mm^2. The semi-transparent current spreading layers to p-GaN were formed by electron beam evaporation of Ni/Au (5/5 nm) on the entire mesa. The epitaxial samples were studied by high resolution X-ray diffraction (HRXRD) and transmission electron microscopy (TEM). The *J-V* characteristics were measured using a Keithley 2410 source meter under the illumination of an

a)E-mail: bzhang@xmu.edu.cn

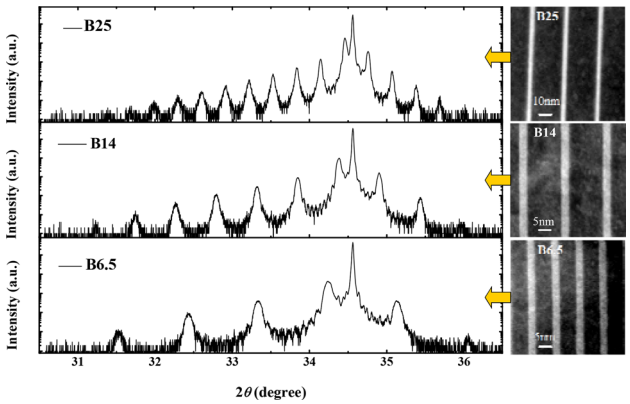

FIG. 1. HRXRD ω-2θ scanning profiles of the (0002) reflection (left) and the corresponding cross-sectional TEM image of the InGaN/GaN MQWs (right) for samples B25, B14, and B6.5. (It is partially extracted from our previous paper.[21])

air-mass 1.5 global solar simulator (AM 1.5, 1 sun). It is noteworthy that the device fabrication processing was mature and the characterization system remained the same as before.[6,8,21]

Figure 1 shows HRXRD ω-2θ scanning profiles of the (0002) reflection (left) for the three samples with different barrier thicknesses. It is clearly observed that there are many well-defined satellite peaks and interference fringes, indicating good interface quality and periodicity in the entire MQW region. This observation is also confirmed by the cross-sectional TEM results (right). Based on the information obtained from HRXRD and TEM measurements, the structural parameters for each sample are determined: the well width of 3.5 nm and barrier thicknesses of about 25 nm, 14 nm, and 6.5 nm for samples B25, B14, and B6.5, respectively. In addition, the average In composition in the three samples is around 25%.

Figure 2 shows *J-V* and *P-V* characteristics of InGaN/GaN MQW-SCs taken at various bias voltages from −10 to 3 V under AM 1.5G solar simulator illumination. J_{sc} increases with reducing the barrier thickness, from 0.111 (B25) to 0.134 (B14) and 0.176 mA/cm^2 (B6.5). There are two reasons: (1) thinner barriers help carriers escape from the quantum well (QW) via tunnelling and contribute more to the photocurrent; (2) a thinner barrier layer implies a weaker polarization electric field (E_p) in the InGaN QW [i.e., decreased tilt (slope) of the energy band for the QW] and it facilitates the collection of photogenerated carriers.[22–24] However, the values of J_{sc} are smaller than the normal case due to the low effective doping in p-GaN ($\sim 7 \times 10^{16}$) and intentionally low Si doping in the

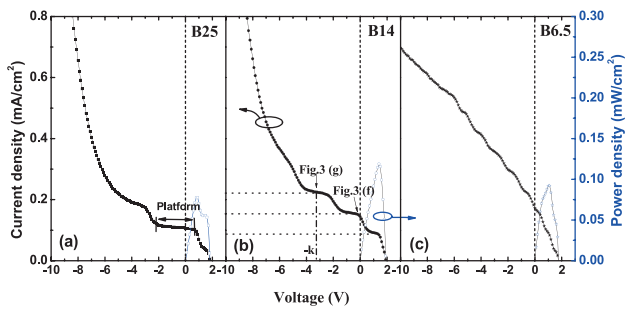

FIG. 2. *J-V* and *P-V* characteristics in the voltage ranging from −10 to 3 V under AM 1.5G solar simulator illumination for InGaN/GaN MQW-SCs.

quantum barrier. The InGaN MQWs can be regarded with coherent growth.[25] If the samples have a strain relaxation, a weaker induced E_p in the QW will result in a stronger net electric field (E_{net}), especially for the sample with a thinner barrier thickness. It can be seen that the relevant characteristics of all the samples will still follow the same variation trend. For the other device performances (V_{oc}, *FF*, conversion efficiency), readers can refer to our previous paper.[21] Although the values were slightly different from those (the mesa size in this study is larger than that reported previously), the change regulation and relevant causes were still the same. With the increasing reverse bias, the current density presents a continual upward tendency and then increases rapidly at a large negative voltage due to the diode breakdown. It is noted that various degrees of inflections (so-called multiple staircases) appear in the *J-V* curve. This abnormal phenomenon results in the reduction of *FF* and conversion efficiency and also some local maximum power points. Actually, the inflection (staircase) behavior has been recorded previously.[11–13] Even so, the work presented here not only shows multiple staircases but also gives some particular interesting regularity: the staircase heights are nearly the same (in the range of $\sim$0.07 mA/cm^2); the staircase platform width decreases for the sample with a thinner barrier, while it slightly increases with the increasing the reverse bias (for the same sample). As such, a deep investigation into the contributing factors and underlying microscopic physical process for this abnormal behaviour is necessary.

In order to get a deeper insight into the device working principle, the internal electric field distribution is first analyzed. Here, the conventional p-i-n SC is used as a reference for comparative analysis. Ideally, if the built-in electric field (E_{bi}) is strong enough, the depletion region will cover the entire intrinsic region. However, due to the high n-type background and insufficient p-type doping in III-nitrides, the depletion region might be narrowed. Then, it will convert to the p-n$^-$-n structure, namely, double-junction diode with p-n$^-$ and n$^-$-n. The n-n$^-$ junction can be ignored since it has a much smaller concentration difference than that of the p-n$^-$ junction. Thus, space charges are thought to mainly distribute near the p-n$^-$ interface and are the same as the electric field, as shown in Figs. 3(c) and 3(e), respectively. Here, the positive direction is defined as the direction along the (0001) orientation. As is well known, III nitride heterojunctions grown on the c-plane have significant polarization interface charges; the resultant E_p is detrimental for the collection of photogenerated carriers.[16,26] As a result, E_{net} ($E_{net} = E_{bi} - E_p$) is reduced and the effective width of the depletion region is further narrowed, as shown in Fig. 3(e) (just for the MQW region). Similarly, the distributions of charges and internal electric field for the above-mentioned MQW-SC are shown in Figs. 3(d), 3(f), and 3(g), respectively. The internal electric field distribution is modulated: E_{net} in the QW is reduced due to the fact that E_p in the well is in the opposite direction [(000-1) orientation] to E_{bi}, while E_{net} in the barrier is increased owing to the same orientation of E_p and E_{bi}. The QW, by contrast, is much more affected by the polarization effect. Thus, once the polarization field is strong enough ($>E_{bi}$), E_{net} in the QW is likely to be reversed to the detrimental direction, i.e., (000-1) orientation.

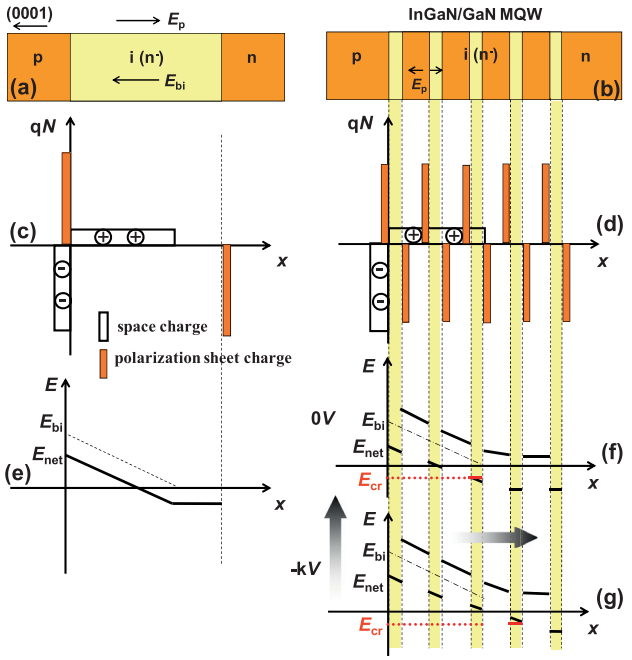

FIG. 3. Schematics of the epitaxial structure for (a) p-i-n and (b) MQW SCs, (c) and (d) the corresponding distribution of space charge and polarization charge, (e)–(g) the corresponding electric-field distribution: (e) and (f) at 0 V and (g) at −k V (k > 0). (E_{bi}, E_p, E_{net}, and E_{cr} are the built-in electric field, polarization-induced electric field, net electric field, and the critical electric field, respectively.)

Figure 3(f) presents a stepwise E_{net} in an imperfect MQW-SC at zero bias, with alternatively up and down and gradually increasing along the (0001) orientation. When the device is reversely biased, E_{net} in the entire MQW region will increase and the depletion region will be widened from the p-type side to the n-type side, owing to the same orientation of the external applied electric field (E_{ext}) and E_{bi}. The carrier escape mechanism from the InGaN QW is via tunneling or thermionic emission, which exhibits field-dependent transport by varying the thickness and height of the barrier.[27] Here, a critical electric field (E_{cr}) (a pseudo parameter) is deemed as a certain E_{net} when the photogenerated carriers happen to escape from the QW. This pseudo parameter is affected by thicknesses of the well and the barrier, E_{net} in the well and the barrier, band offset, material quality, etc. Thus, reversing the applied voltage will make E_{net} of some QWs (i.e., $<E_{cr}$) reach or exceed E_{cr}, as is evident from Figs. 3(f) and 3(g), which show the E_{net} distributions at 0 V and −k V (k > 0), respectively, and the corresponding current is schematically marked in Fig. 2(b). This microscopic physical process in the MQW region proceeds along the (000-1) orientation one by one, leading to a step-by-step increase in the photocurrent, just like the "staircase" shown in Fig. 2. That is why all the platform heights show a value of about 0.07 mA/cm^2, from which the numbers of photogenerated electron-hole pairs for each QW can be estimated, i.e., ∼4.375 × 10^{12} (mm^{-2} s^{-1}). In addition, for the device with a thicker barrier or a wider depletion region, a larger increment of voltage is required, as evidenced by the staircase platform broadening with the increasing barrier thickness or reverse bias voltage (Fig. 2). Based on the information of the staircase-like *I-V* curve, the one-period thickness of InGaN/GaN MQW (D) can be estimated as the variation of the depletion width in the intrinsic region under the corresponding applied biases (V_1, V_2) of the one-period staircase. The equation of the depletion width (W) as a function of applied bias (V) is $W(V) = W_0(1 - V/V_{bi})^{1/2}$, where V_{bi} and W_0 are the built-in voltage across the p-n junction and the depletion width at equilibrium and defined as $V_{bi} = (kT/q)\ln(N_A N_D/n_i^2)$ and $W_0 = [2\varepsilon_s V_{bi}(N_A + N_D)/qN_A N_D]^{1/2}$, respectively.[28] The relative permittivity (ε_s) of GaN is 8.9; the doping concentrations of the donor (N_D) and acceptor (N_A) are 2.5 × 10^{17} cm^{-3} and 7 × 10^{16} cm^{-3}, respectively; n_i is the intrinsic concentration of $In_{0.25}Ga_{0.75}N$ at 300 K. Then, the one-period thickness of MQW is obtained: $D = N_A/(N_A + N_D) \times [W(V_2) - W(V_1)]$. The calculated values are 30.1, 18.3, and 8.6 nm for samples B25, B14, and B6.5, respectively, which almost agree with the corresponding characterization results of 28.5, 17.5, and 10 nm.

E_{net} is closely related to E_{bi}, E_{ext}, and E_X (additional electric fields induced by other special cases) and is equal to the vector sum of each component, $\boldsymbol{E}_{net} = \boldsymbol{E}_{bi} + \boldsymbol{E}_{ext} + \boldsymbol{E}_X$. If we designate the direction of $\boldsymbol{E}_{bi}$ as "positive," the above vector expression can be simplified algebraically, as illustrated in Fig. 4. Ideally (assuming no resistance and no other negative factors), a normal *I-V* curve [Fig. 4(a)] can be obtained when E_{bi} is strong enough: (1) at zero bias (point B), almost all the photogenerated carriers can be driven by E_{bi} (also called drift current, I_{dri}), mainly contributing to the photocurrent (I_p); (2) at reverse bias (point A), E_{net} is equal to $E_{bi} + E_{ext}$ due to the same orientation of them, producing a higher tilt (slope) of the energy band for the intrinsic region (i-region inset), thereby enhancing the collection of photogenerated carriers;

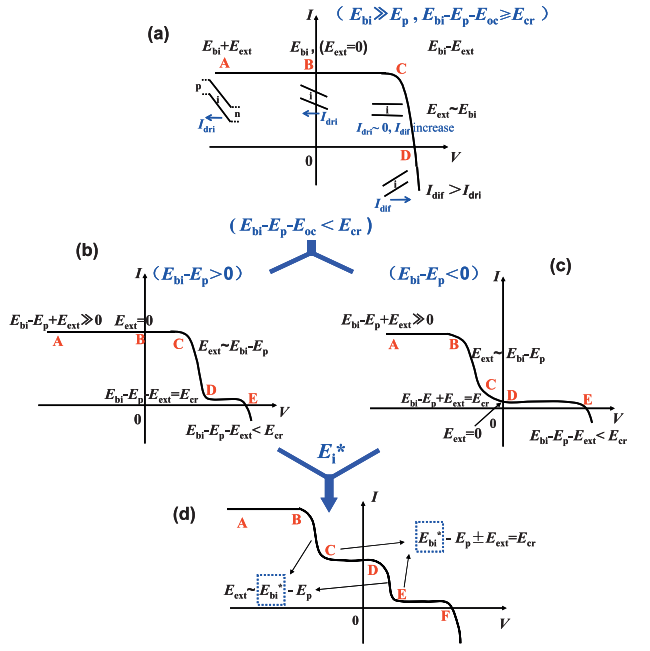

FIG. 4. Schematics of *I-V* curves under different conditions: (a) the normal case; (b) inflection in the first quadrant; (c) inflection in the second quadrant; and (d) the multiple staircases. Insets show the corresponding electric-field conditions and schematic alignment of energy levels for the intrinsic region. (E_{bi}, E_p, E_{ext}, E_{oc}, E_i^*, and E_{cr} are the built-in electric field, polarization-induced electric field, external applied bias electric field, electric field induced by the applied bias of V_{oc}, spatially stepwise varying electric field, and the critical electric field, respectively. I_{dif} and I_{dri} are the diffusion and drift currents, respectively.)

(3) at small forward bias (between points B and C), E_{net} is equal to $E_{bi} - E_{ext}$ due to their opposite orientations, while I_p remains constant until E_{ext} is comparable to E_{bi} (point C); (4) with increasing forward bias, diffusion current (I_{dif}) increases and I_{dri} decreases rapidly (between points C and D), since the flattening energy band implies a weak driven force for the carrier collection; (5) with further increasing forward bias, a reversed E_{net} even appears ($E_{bi} < E_{ext}$, reversed tilt of the energy band), resulting in a huge loss of photogenerated carriers in the recombination, and consequently, the *I-V* characteristic after point D is dominated by a large amount of I_{dif}, namely, the dark injection current (contrary to I_{dri}).

As for the InGaN/GaN solar cell, E_{net} in the i-region is also influenced by E_p that plays a negative role in weakening the internal electric field and thus is equivalent to $E_{bi} - E_p$ for the InGaN layer. If E_{bi} is large enough ($E_{bi} \gg E_p$), the influence of E_p can be ignored. Likewise, if there exists $E_{bi} - E_p - E_{oc} \geq E_{cr}$ (E_{oc}-an equivalent electric field induced by the applied bias of V_{oc} and E_{cr}-a critical electric field mentioned above), the resultant E_{net} can be still sufficient for the collection of photogenerated carriers. In general, the normal *I-V* curve can be obtained in the above two conditions [Fig. 4(a)]. For $E_{bi} - E_p - E_{oc} < E_{cr}$, however, the "inflection" will appear in the *I-V* curve for a certain bias voltage, which involves the following two cases:

(i) If $E_{bi} - E_p > 0$, the inflection might appear in the first quadrant as shown in Fig. 4(b). Making reference to Fig. 4(a), point A in Fig. 4(b) corresponds to E_{net} that is far greater than zero, i.e., $E_{bi} - E_p + E_{ext} \gg 0$. However, when the applied bias reaches a certain value (E_{ext} comparable with $E_{bi} - E_p$), the carrier collection probability will reduce rapidly, resulting in higher recombination in the i-region and consequently a dramatic drop of I_p in the first quadrant (range CD). The inflection point D is a critical state ($E_{bi} - E_p - E_{ext} = E_{cr}$), where photogenerated carriers would happen to escape from restriction and contribute to the terminal I_p. After point D (range DE), where E_{net} is smaller than E_{cr} in this region [$E_{bi} - E_p - E_{ext} < E_{cr}$, Fig. 4(b)], I_p remains almost constant until injection becomes dominant.

(ii) If $E_{bi} - E_p < 0$, E_{net} could be larger than E_{cr} when negative voltage is applied. As such, the inflection will shift to the second quadrant [Fig. 4(c)]. Based on analyses in Fig. 4(b), one has no difficulty in understanding this figure.

Apart from the above-mentioned cases, a non-uniform internal electric field may be present in the absorption region, for example, the region-related stepped E_{net} [shown in Fig. 3(f)], here denoted as E_i^*. With applying negative voltage, the depletion region will be widened and the entire E_{net} will increase. Thus, the regional E_{net} will be larger than E_{cr} in turn [Figs. 3(f) and 3(g)]. In this case, photogenerated carriers can be collected from QW by QW, leading to multiple-step transitions in I_p, as shown in Figs. 4(d) and 2. As mentioned in Fig. 3, the platform width of the above staircase shape is directly related to the barrier thickness and the external bias.

From the above analyses, we can conclude that if E_{net} is strong enough and every period of MQW is almost the same, the MQW-SC could be regarded as a single QW-SC with a normal *I-V* curve, where I_p can be equal to that of single QW multiplied with the number of QWs. However, if E_{net} is not strong enough, the MQW region will not be completely depleted, and a non-uniform internal electric field is generated. In this case, the QWs contribute to I_p one by one with the increasing reverse bias voltage. Since I_p is a superposition of each QW under various bias voltages, the abnormal behaviour of "staircase" will appear in the *I-V* curve. Besides the above-mentioned E_p, any factor that can reduce the E_{net} is probable to cause inflection in the *I-V* curve, such as insufficient p-type doping, high n-type background, and significant polarization effect. There is no doubt that the inflection behaviour is also relevant to the special epitaxial structure, for example, the MQW. Through analysis of the *I-V* curve, it would be hopeful to get more insight into the device problems, thereby promoting the epitaxial design and fabrication process.

In summary, InGaN/GaN MQW-SCs with different barrier thicknesses were investigated, and the abnormal feature of the staircase in the *I-V* curve was analyzed in detail. It is demonstrated that the thinner barrier helps the transport of photogenerated carriers. However, due to the insufficient p-type doping, significant polarization effect, and high n-type background, the MQW region is not completely depleted and a spatially stepwise varying internal field mainly distributes near the p-side. With reversing the bias voltage, the carriers will be driven by the increased E_{net} QW by QW along the (000-1) direction, thereby resulting in the occurrence of the staircase-like feature in the *I-V* curve. Furthermore, we qualitatively analyze the internal field of the solar cell and give the formation conditions of the *I-V* curve with various types of inflections. Hopefully, the results help to improve the device design and fabrication process, and the analytical methods are also applicable to other types of solar cells.

This work was supported by the National Natural Science Foundation of China (Nos. 61404059 and U1505253) and the Training Program for Distinguished Young Scholars in Fujian Province University (No. B16163, Minjiaoke [2016] No. 23).

[1]H. Hamzaoui, A. Bouazzi, and B. Rezig, Sol. Energy Mater. Sol. Cells **87**(1–4), 595–603 (2005).
[2]J. Wu, J. Appl. Phys. **106**(1), 011101 (2009).
[3]J. Wu, W. Walukiewicz, K. M. Yu, W. Shan, J. W. Ager III, E. E. Haller, H. Lu, W. J. Schaff, W. K. Metzger, and S. Kurtz, J. Appl. Phys. **94**(10), 6477–6482 (2003).
[4]A. De Vos, Energy Convers. **16**(1–2), 67–78 (1976).
[5]D. Cherns, S. Henley, and F. Ponce, Appl. Phys. Lett. **78**(18), 2691–2693 (2001).
[6]X. M. Cai, S. W. Zeng, and B. P. Zhang, Appl. Phys. Lett. **95**, 173504 (2009).
[7]R. Dahal, B. Pantha, J. Li, J. Lin, and H. Jiang, Appl. Phys. Lett. **94**, 063505 (2009).
[8]X. M. Cai, Y. Wang, B. H. Chen, M. M. Liang, W. J. Liu, J. Y. Zhang, X. Q. Lv, L. Y. Ying, and B. P. Zhang, IEEE Photonics Technol. Lett. **25**(1), 59–62 (2013).
[9]W. Götz, N. Johnson, J. Walker, D. Bour, and R. Street, Appl. Phys. Lett. **68**, 667 (1996).
[10]R. R. Lieten, V. Motsnyi, L. Zhang, K. Cheng, M. Leys, S. Degroote, G. Buchowicz, O. Dubon, and G. Borghs, J. Phys. D: Appl. Phys. **44**(13), 135406 (2011).

[11]C. J. Neufeld, S. C. Cruz, R. M. Farrell, M. Iza, J. R. Lang, S. Keller, S. Nakamura, S. P. DenBaars, J. S. Speck, and U. K. Mishra, Appl. Phys. Lett. **98**, 243507 (2011).
[12]R. Dahal, J. Li, K. Aryal, J. Lin, and H. Jiang, Appl. Phys. Lett. **97**, 073115 (2010).
[13]S.-B. Choi, J.-P. Shim, D.-M. Kim, H.-I. Jeong, Y.-D. Jho, Y.-H. Song, and D.-S. Lee, Appl. Phys. Lett. **103**(3), 033901 (2013).
[14]H.-W. Wang, C.-C. Hsieh, F.-I. Lai, S.-H. Lin, and H.-C. Kuo, in paper presented at the 2013 IEEE 39th Photovoltaic Specialists Conference (PVSC), 2013.
[15]Z. Q. Li, M. Lestradet, Y. G. Xiao, and S. Li, Phys. Status Solidi A **208**(4), 928–931 (2011).
[16]J.-Y. Chang and Y.-K. Kuo, IEEE Electron Device Lett. **32**(7), 937–939 (2011).
[17]Y.-C. Yao, M.-T. Tsai, C.-Y. Huang, T.-Y. Lin, J.-K. Sheu, and Y.-J. Lee, Appl. Phys. Lett. **103**(19), 193503 (2013).
[18]C. A. Fabien and W. A. Doolittle, Sol. Energy Mater. Sol. Cells **130**, 354–363 (2014).
[19]S. Lee, Y. Honda, and H. Amano, J. Phys. D: Appl. Phys. **49**, 025103 (2016).
[20]M. Sumiya, T. Honda, L. Sang, Y. Nakano, K. Watanabe, and F. Hasegawa, Phys. Status Solidi A **212**(5), 1033–1038 (2015).
[21]X. M. Cai, X. Q. Lv, X. J. Huang, X. L. Wang, M. S. Wang, L. Yang, H. L. Zhu, and B. P. Zhang, Phys. Status Solidi A **215**, 1700581 (2018).
[22]J. Wierer, D. Koleske, and S. Lee, Appl. Phys. Lett. **100**(11), 111119 (2012).
[23]N. Watanabe, H. Yokoyama, N. Shigekawa, K. Sugita, and A. Yamamoto, Jpn. J. Appl. Phys. **51**(10), 10ND10 (2012).
[24]R. Luca, M. Anna, A. Akhil, N.-C. Arántzazu, V.-F. Sirona, B. Joël, D. Christophe, E. Joël, and M. Eva, Jpn. J. Appl. Phys. **54**(7), 072302 (2015).
[25]S. Pereira, M. R. Correia, E. Pereira, C. Trager-Cowan, F. Sweeney, K. P. O'Donnell, E. Alves, N. Franco, and A. D. Sequeira, Appl. Phys. Lett. **81**(7), 1207–1209 (2002).
[26]J. Wierer, Jr., A. Fischer, and D. Koleske, Appl. Phys. Lett. **96**, 051107 (2010).
[27]J. Lang, N. Young, R. Farrell, Y. R. Wu, and J. Speck, Appl. Phys. Lett. **101**(18), 181105 (2012).
[28]A. Luque and S. Hegedus, *Handbook of Photovoltaic Science and Engineering* (Wiley, Chichester, 2003).